HHS Public Access

Author manuscript

Environ Sci Technol. Author manuscript; available in PMC 2018 June 11.

Published in final edited form as:

Environ Sci Technol. 2017 June 20; 51(12): 6802–6811. doi:10.1021/acs.est.7b01536.

Ambient Size Distributions and Lung Deposition of Aerosol Dithiothreitol-Measured Oxidative Potential: Contrast between Soluble and Insoluble Particles

Ting Fang[†], **Linghan Zeng**[†], **Dong Gao**[‡], **Vishal Verma**[§], **Aleksandr B. Stefaniak**[⊥], and **Rodney J. Weber**[*,†]

[†]School of Earth and Atmospheric Sciences, Georgia Institute of Technology, Atlanta, Georgia 30332, United States

[‡]School of Civil and Environmental Engineering, Georgia Institute of Technology, Atlanta, Georgia 30332, United States

[§]Department of Civil and Environmental Engineering, University of Illinois Urbana–Champaign, Champaign, Illinois 61801, United States

[⊥]Respiratory Health Division, National Institute for Occupational Safety and Health, Morgantown, West Virginia 26505, United States

Abstract

Ambient particulate matter may upset redox homeostasis, leading to oxidative stress and adverse health effects. Size distributions of water-insoluble and water-soluble OP^{DTT} (dithiothreitol assay, measure of oxidative potential per air volume) are reported for a roadside site and an urban site. The average water-insoluble fractions were 23% and 51%, and 37% and 39%, for fine and coarse modes at the roadside and urban sites, respectively, measured during different periods. Water-soluble OP^{DTT} was unimodal, peaked near 1–2.5 μm due to contributions from fine-mode organic components plus coarse-mode transition metal ions. In contrast, water-insoluble OP^{DTT} was bimodal, with both fine and coarse modes. The main chemical components that drive both fractions appear to be the same, except that for water-insoluble OP^{DTT} the compounds were absorbed on surfaces of soot and non-tailpipe traffic dust. They were largely externally mixed and deposited in different regions in the respiratory system, transition metal ions predominately in the upper regions and organic species, such as quinones, deeper in the lung. Although OP^{DTT} per mass (toxicity) was highest for ultrafine particles, estimated lung deposition was mainly from accumulation and coarse particles. Contrasts in the phases of these forms of OP^{DTT} deposited in the respiratory system may have differing health impacts.

[*]Corresponding Author: Phone: (404) 894-1750; fax: (404) 894-5638; rodney.weber@eas.gatech.edu.

ORCID

Ting Fang: 0000-0002-4845-2749

Notes

The authors declare no competing financial interest.

Supporting Information

The Supporting Information is available free of charge on the ACS Publications website at DOI: 10.1021/acs.est.7b01536.

Tables S1–S7, Figures S1–S10, methods for dividing deposits between cut filter portions and OCEC analysis, equations to fit the distribution, and methods to measure total DTT activity on MOUDI filters (PDF)

Graphical Abstract

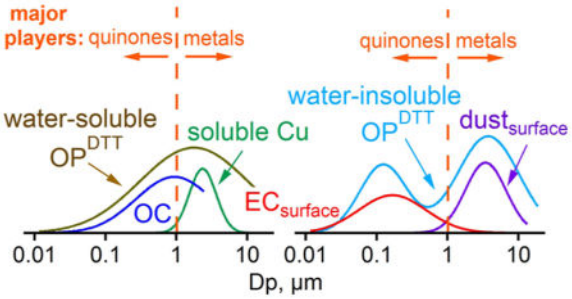

INTRODUCTION

Studies have associated exposure to particulate matter (PM) with adverse health effects.[1–3] Oxidative stress, an imbalance toward an excess of reactive oxygen species (ROS), is considered to induce inflammation, a possible mechanism leading to adverse health effects.[4] In an effort to find a more biologically relevant metric than bulk PM mass concentration to represent the integrated effects from multiple toxic components in PM, oxidative potential (OP), defined as the capability of particles to deplete physiological antioxidants (reductants) and generate ROS, has been proposed. Positive associations between cardiorespiratory health end points and OP measured with the dithiothreitol (DTT) assay (OP^{DTT}) have been reported (units for OP^{DTT} are loss of DTT per time per volume of air sampled).[5–7] Physiologically relevant assays, glutathione (OP^{GSH}) and ascorbic acid (OP^{AA}) (both antioxidants found in lung fluid), tested in a synthetic respiratory tract lining fluid model, show mixed results; OP^{GSH} has been associated with lung cancer mortality[8] and myocardial infarction,[9] while OP^{AA} was not. In other studies, neither OP^{GSH} nor OP^{AA} was associated with respiratory function[10,11] or cardiorespiratory mortality.[12] Comparing OP^{DTT} and OP^{AA}, we found positive associations between asthma/wheezing and congestive heart failure with OP^{DTT}, but not with OP^{AA}.[13] Here, we focus on OP^{DTT}, but the analysis could be repeated for other OP assays.

In many cases, when implementing the DTT assay, particles are extracted in water followed by liquid filtration to remove solid or insoluble fractions. But studies show that OP^{DTT} can also be associated with insoluble aerosol components. Daher et al.[14] found that the OP^{DTT} values of particles collected using a Biosampler without filtration, thought to collect both water-soluble and insoluble fractions, were substantially higher than those of the aqueous extracts of the particles collected with a filter. McWhinney et al.[15] found that approximately 25% and 90% of the OP^{DTT} was in the water-insoluble fraction for urban PM and diesel exhaust particles, respectively. These studies and others[16–18] provide evidence that insoluble aerosol species contribute to OP and should be considered when assessing health effects.

Elemental carbon (EC, black carbon or soot) is one of the insoluble species in PM identified as a serious health hazard. Research has shown that exposure to soot exacerbates cardiovascular and respiratory symptoms.[19–21] Soot is usually found mainly in the fine mode ($PM_{2.5}$, meaning all particles with aerodynamic diameter less than 2.5 μm) and is a product

of incomplete combustion.[22] In terms of OP, studies have linked reactive oxygen intermediates formed on the surface of soot, such as quinones from oxidation of polycyclic aromatic hydrocarbons (PAHs) by ozone, to increased OP^{DTT}.[23,24] Both representative[16] and real[15,25] diesel exhaust soot, when oxidized by ozone, exhibited much higher OP^{DTT}. The OP^{DTT} associated with diesel exhaust soot was not extractable by acid[26] or organics solvents, including methanol[15] and dichloromethane (DCM),[15,26] indicating that the DTT-active species were strongly adsorbed to the soot surface. Association between OP^{DTT} and the number of surface sites on nanoparticles[27] has been reported. These laboratory findings indicate that OP^{DTT} is contiguous with the surface of soot, and that OP^{DTT} may play a key role in the adverse health effects of soot. Soot also provides a surface for the formation and stabilization of some ROS, e.g., "environmentally persistent free radicals" (EPFRs),[28,29] which may also be related to soot toxicity.

Coarse-mode aerosol ($PM_{2.5–10}$, meaning particles with a size between 2.5 and 10 μm) also has been linked to adverse health effects,[30–32] and a significant fraction of the coarse-mode particle species are insoluble, remaining solid when deposited in liquid environments. Although variable levels of soot can be found in particles larger than $PM_{2.5}$, most insoluble species are associated with mechanically generated aerosols, such as mineral and fugitive dust. In urban environments, this has been linked to tire/brake wear components from traffic and construction activities in non-arid regions.[33–35] Minerals (e.g., silicates, calcium carbonates, metal oxides, or clay minerals[36]) can induce ROS formation as a solid particle binding to a cell surface or entering the cell by engulfment and lead to ROS production, or as a "carrier" of more toxic species such as metals and surface-sorbed PAHs.[37]

Aerodynamic size, in part, affects the location of deposition in the respiratory system.[38,39] Particles deposited deep within the lung are most damaging due to difficulty in clearance and more readily enter the bloodstream when deposed in the alveoli.[40,41] The circulatory system translocates soluble species and insoluble particles and the associated OP from the lung to other critical organs such as kidneys,[42,43] heart,[42] and liver,[42–44] among others,[43] causing localized effects. In addition, recent studies show that particles deposited in the nasal region translocate into the central nervous system via the olfactory bulb and cause brain lesions, dementia[45–47] and impaired cognitive development.[48] Particle size is also related to different toxic effects. Various studies have attempted to link PM size to adverse health effects. Some studies indicate that coarse particles are more potent at inducing hemolysis and DNA degradation,[31] and pro-inflammatory cytokines in vitro[32] than fine particles ($PM_{2.5}$), whereas some show that inhibition of cell proliferation is significantly stronger by $PM_{2.5}$.[31] The ultrafine fraction ($PM_{0.1}$) is often viewed as highly toxic. $PM_{0.1}$ is observed to cause airway inflammation in vivo,[49] more strongly associated with biomarkers of systemic inflammation than larger-size fractions,[50] and the small size enables penetration of pulmonary barriers and travel to other organs or cell membranes leading to damage of cell organelles, such as mitochondria,[51] whereas accumulation ($PM_{0.1–2.5}$) and coarse fractions do not show similar behaviors; however, more recent studies show that solid particles up to 1.75 μm in diameter also translocate to various organs from the lung.[43]

Although there has been substantial research on the toxicity of ambient PM in relation to particle size, there are limited studies on the ambient size distribution of OP. Several

studies[51–54] have examined the OP^{DTT} of different size fractions of PM collected by the Versatile Aerosol Concentration Enrichment System (VACES), contrasting OP between broad aerosol modes, e.g. quasi-ultrafine (aerodynamic diameter, $D_p < 0.18\ \mu m$), accumulation ($0.18 \leq D_p \leq 2.5\ \mu m$), and coarse fractions ($D_p > 2.5\ \mu m$). It is generally found that, on a per unit air volume basis, accumulation-mode particles have the highest OP^{DTT} per volume air, whereas ultrafine particles show much higher OP^{DTT} per unit mass than accumulation and coarse particles.

Here, we investigate the ambient size distribution and the major chemical players of both water-soluble and -insoluble OP^{DTT} for particles collected from two contrasting sites. Specifically, we study the relationship between fine-mode soot and coarse-mode dust and water-insoluble OP^{DTT}. The size distributions of OP were also used to assess the deposition of both forms of OP^{DTT} in the human respiratory system.

MATERIALS AND METHODS

Size-Segregated Sampling of PM

Details on the sampling and chemical analysis can be found in Fang et al.[55] Two 10-stage Micro-Orifice Uniform Deposit Impactors (MOUDI, MSP Corp., Shoreview, MN, USA) were used to collect size-segregated ambient particles at a roadside (RS) site and an urban representative (GT) site in Atlanta, GA, from summer 2015 to spring 2016. The RS site was adjacent to highly congested interstate highway (I75/85), and the GT site was located on the rooftop of a building on the Georgia Tech campus, roughly 420 m from the RS site. The 50% cutoff aerodynamic diameters of the MOUDI are 18, 10, 5.6, 3.2, 1.8, 1.0, 0.56, 0.32, 0.18, 0.1, and 0.056 μm. The MOUDIs were operated in a non-rotating mode without a back-up filter at a flow rate of 30 L min^{-1}. Methods to account for non-uniform deposits of particles due to non-rotating mode on chemical analysis are described in the supplement. Fourteen MOUDI samples were collected (seven at each site), while four from these samples (i.e., two pairs) were collected simultaneously at both sites. For each MOUDI run, sampling was conducted under ambient RH and temperature (MOUDIs located outdoors) for approximately 7 days to provide sufficient mass loadings for various analyses. Studies on the stability of OP at ambient temperature are currently lacking, but Sauvain et al.[56] found that OP^{DTT} of particles collected on Teflon filters were stable after about 170 h (~7 days), indicating a 7-day sampling period will not significantly affect OP^{DTT}. All OP analyses in this work were done after a maximum of 3-day sample storage in sealed Petri dishes at −18 °C. Sampling periods, filter types used, and species quantified are summarized in Table S1. For every MOUDI sample, one field blank was included. All data were blank corrected with the averages from all blanks combined. Consistency between the two MOUDIs was first assessed by comparing water-soluble OP^{DTT} (OP^{DTT}_{WS}) when operated simultaneously at the GT site. Orthogonal regression yielded a slope of 1.0 ± 0.1 (value ± one standard deviation), low intercept ($-6.0 \times 10^{-5} \pm 0.002$ nmol min^{-1} m^{-3}), and high r^2 (0.92) (Figure S1).

Chemical Components Analysis

Teflon (47 mm PTFE Membrane Filters, 2 μm pore size, Pall Corp., Ann Arbor, MI, USA) and quartz filters (47 mm, Tissuquartz Filters, Pall Corp., Ann Arbor, MI, USA) were used as impaction surfaces, depending on the chemical analyses. For simultaneous sets, Teflon filters were used for one MOUDI at each site; for different-day collection, both quartz and Teflon filters were used for two MOUDIs at one site. Along with OP^{DTT}, particle chemical components measured included organic carbon (OC), elemental carbon (EC), ions, water-soluble, and total metals. OC, EC, ions, and metals were measured on quartz filters, and OP^{DTT} was measured on Teflon filters. OC and EC were measured using a Sunset OCEC Analyzer (Sunset Laboratory Inc., Tigard, OR) following the IMPROVE protocol.[57] Water-soluble and total metals, including copper, manganese, and iron, were measured using inductively coupled plasma mass spectrometry (ICP-MS) (Agilent 7500a series, Agilent Technologies, Inc., CA, USA). For water extracts, filters were sonicated in deionized (DI) water (>18 MΩ cm^{-1}) with an Ultrasonic Cleanser (VWR International LLC, West Chester, PA, USA) for half an hour, and filtered with PTFE 0.45 μm syringe filters (Fisherbrand). For determining total metals (elemental), filters were first digested in 2 mL of 1:3 HNO_3:HCl solution, diluted in DI water to a final volume of 10 mL, and then filtered with 0.45 μm syringe filters. Both water-soluble and total samples were then acidified by adding HNO_3 to achieve a final concentration of 2% HNO_3. A 25 ppb internal standard of scandium was added to every sample to monitor analytical drift. Only Cu data are discussed since our previous studies[13,58] show Cu is the main transition metal contributing to the OP^{DTT}. Ions were determined on the water-extracted samples (filtered with 0.45 μm filters) using ion chromatography (Metrohm 761 Compact ICs, Riverside, FL, USA). Surface area size distributions of OC, EC, and $CaCO_3$ were calculated assuming spherical particles and the same density across all size ranges using the following equation:

$$\frac{dn_s}{d\ln D_p} = \frac{6}{\rho D_{pg} 10^6} \times \frac{dn_m}{d\ln D_p} \quad (1)$$

where $\frac{dn_s}{d\ln D_p}$ and $\frac{dn_m}{d\ln D_p}$ are the surface area and mass distribution functions, respectively; D_p is aerodynamic diameter (μm); D_{pg} is the geometric mean diameter of each MOUDI stage (the square root of the product of upper and lower D_p of each MOUDI stage, μm); 10^6 is the unit conversion factor; and ρ is the particle density (1.27 g cm^{-3} for OC,[59] 1.77 g cm^{-3} for EC,[59] and 2.71 g cm^{-3} for $CaCO_3$). [$CaCO_3$ was calculated from Ca^{2+}, although the $CaCO_3$ concentration is likely underestimated since only water-soluble Ca^{2+} was measured and $CaCO_3$ is not highly soluble. $CaCO_3$ is taken as a surrogate of mineral dust,[60,61] and the shape of the $CaCO_3$ surface area distribution is taken to be identical as ambient mineral dust distribution.] The surface area size distribution of OC, EC, and $CaCO_3$ can be found in Figure S2.

Oxidative Potential (OP)

OP measurement on Teflon MOUDI filters include OP_{ws}^{DTT} and total DTT (OP_{total}^{DTT}) activities. Water-insoluble OP^{DTT} was determined by difference ($OP_{wi}^{DTT} = OP_{total}^{DTT} - OP_{ws}^{DTT}$). The DTT assay was conducted manually or by a semi-automated instrument[13,62] on the filtered DI water extracts to determine OP_{ws}^{DTT}. A 1 mM DTT solution was added to the sample extract with potassium phosphate buffer (Kbuffer, pH = 7.4) at 37 °C. At five different specific time intervals, a small aliquot from the mixture was withdrawn to determine remaining DTT concentration with a light absorption method. DTT consumption rate was used to calculate final OP. The DTT analysis explicitly followed the method described by Cho et al.[53]

OP_{total}^{DTT} was determined manually with the same method as that for OP_{ws}^{DTT}, except that the extract was not filtered. The sample filter was also left in the sample-Kbuffer-DTT mixture such that the DTT-active species from insoluble particles suspended in the extracts, and those still on the filter surface, could be in contact with added DTT and consume DTT over time. That is, after 0.5-h sonication, Kbuffer and DTT (1 mM) were added to the extract with the sample filter included. At five time intervals, a small aliquot was withdrawn to determine remaining DTT concentration using the same light absorption method as stated above. A detailed method for measuring OP_{total}^{DTT} can be found in the supplement. The consistency of the manual DTT method was monitored with 9,10-phenanthra-quinone as a positive control run on different days with the samples ($N = 10$, coefficient of variation <10%). Lognormal distributions were fit to all data. Fit equations are summarized in the supplement. For OP, geometric mean diameters (GMD) and geometric standard deviation (σ_g), total OP, and the associated uncertainties for each MOUDI set can be found in Tables S2–S4. Tables S2–S4 also give the overall combined mean GMD and σ_g for both measures of OP at the RS and GT sites. This mean GMD and σ_g were used to calculate the averaged frequency distribution ($df/d\ln D_p$) of OP at each site. Average distribution ($d\,OP/d\ln D_p$) was calculated differently. Each stage of the average distribution was the mean of corresponding stages from all MOUDI samples. The MOUDI sets collected in summer 2015 had a different cutoff diameter of 2.5 μm instead of a standard cutoff diameter of 1.8 μm; for these MOUDI sets, only stages with the same cutoff diameters as other MOUDI samples were included in calculating the average distribution. All OP^{DTT} reported is in units of DTT loss rate per volume of air.

Intrinsic OP was calculated by dividing measured OP with PM mass concentration. Given that direct mass measurement was not done, PM mass concentration for each MOUDI stage was estimated from the sum of measured chemical components, including elemental carbon (EC), organic mass (OC*1.6),[59] total metals, and ions (SO_4^{2-}, NO_3^-, Cl^-, and NH_4^+). Total metals were represented by their oxide forms (K_2O, $CaCO_3$, MgO, CuO, MnO_2, and Fe_2O_3), except elemental mass was used for Cu and Mn for stages below 1.8 μm, given that Cu and Mn particles smaller than 1.8 μm are mostly water-soluble[55] and, studies show, likely in the form of metal sulfates (and sulfate was measured).[63,64] The PM mass distributions for both sites can be found in Figure S3.

Modeling Deposition in the Human Respiratory System

Deposition efficiency in the human respiratory tract represents the mean probability of an inhaled particle being deposited in a given compartment. Particle deposition efficiency estimates are based on empirical expressions derived from human inhalation data (ICRP, 1994).[65] Deposition was modeled for an adult male at light work (breathing rate = 1.5 m^3 h^{-1}, respiration frequency = 20 min^{-1}, and tidal volume = 1250 cm^3) assuming unit density spherical particles (i.e., 1 g cm^{-3}). Regional deposition in different compartments of the respiratory tract (extrathoracic, bronchial, and alveolar regions) were calculated for nose-only breathing and are summarized in Figure S4. Deposition of OP in the respiratory system was obtained by multiplying the averaged frequency distributions of OP with the deposition efficiency. OP deposition was integrated over three particle size modes (ranges): quasi-ultrafine (<0.18 μm), accumulation (0.18–3.2 μm), and coarse (3.2–18 μm). Only total, alveolar, and extrathoracic deposition are discussed.

RESULTS AND DISCUSSION

Soluble Fraction and Size Distribution of Particulate Oxidative Potential

Figure 1 shows the size distribution of OP_{ws}^{DTT} and OP_{total}^{DTT}; the difference is OP_{wi}^{DTT}. The OP_{wi}^{DTT} to OP_{total}^{DTT} fraction depended on particle size. Average OP_{wi}^{DTT} to OP_{total}^{DTT} ratios at the RS site were 23% and 51% in the fine and coarse mode, respectively. Average insoluble fraction at the GT site were similar in the fine (37%) and coarse (39%) mode. Note that these ratios were averaged from all MOUDI data.

Frequency distributions are plotted to compare shapes of OP distributions for all MOUDI data, since they are independent of the ambient OP levels, which can vary substantially between sites and measurement periods. Log-normal fitted frequency distribution for individual MOUDI measurement ($N = 5$ for OP_{ws}^{DTT}, and $N = 2$ for OP_{wi}^{DTT}) at RS and GT sites and the average frequency distribution of OP are shown in Figure 2 for OP_{ws}^{DTT} and OP_{wi}^{DTT}.

OP_{wi}^{DTT} had a bimodal distribution with a peak in the accumulation and coarse modes, in stark contrast to OP_{ws}^{DTT}, which was unimodal with peak near the minimum between the two OP_{wi}^{DTT} modes (geometric mean diameter, GMD, ranged from 0.80 to 2.51 μm at both sites, Table S2). The sources and/or atmospheric processes producing OP_{ws}^{DTT} and OP_{wi}^{DTT} clearly differ.

Contrasting the OP frequency distributions at the two sites provides insights on the contributions of highway emissions to OP_{ws}^{DTT} and OP_{wi}^{DTT}. Small variations were observed in OP_{ws}^{DTT} frequency size distributions (Figure 2), especially at the GT site. OP_{ws}^{DTT} from one MOUDI sample collected in fall at the RS site, however, showed a peak at a much larger size (GMD = 2.51 μm) than the average frequency distribution (GMD_{mean} = 1.46 μm),

suggesting that roadside OP_{ws}^{DTT} was occasionally affected largely by non-tailpipe traffic sources, which pushed the GMD to a larger size range. When removing this measurement, the GMD_{mean} for OP_{ws}^{DTT} at the RS site was 1.20 μm, much closer to that at the GT site, showing that OP_{ws}^{DTT} had a more regional character, consistent with earlier findings in the same region.[58,62] For OP_{wi}^{DTT}, the coarse-mode peak was larger than the accumulation mode at the RS site, while the opposite was observed at the GT site, indicating coarse-mode OP_{wi}^{DTT} was more affected by non-tailpipe traffic emissions. More limited transport of large size particles due to sedimentation, resulting in lower OP_{wi}^{DTT} at the GT site also would play a role.

Comparing simultaneous measurements at the two sites (Figure 3) supports the above inferences. For example, OP_{wi}^{DTT} collected simultaneously at both sites exhibited much higher coarse mode levels at the RS site than at the GT site, suggestive of a major contribution from non-tailpipe traffic emissions to coarse-mode OP_{wi}^{DTT}. Accumulation-mode OP_{wi}^{DTT} and OP_{ws}^{DTT} levels were similar at both sites, indicating mainly a regional influence on accumulation-mode OP_{wi}^{DTT} and OP_{ws}^{DTT} for these MOUDI data sets.

Sources and Processes Based on Other Measured Species

Figure 4 shows the ambient size distributions of OP_{wi}^{DTT} and OP_{ws}^{DTT}, OC, EC, Ca^{2+}, and water-soluble Cu, and the estimated surface area distributions of EC and $CaCO_3$ at both sites. Ambient size distributions of chemical species provide clues to the sources and processes that led to the observed OP distributions. Fang et al.[55] has reported on particle size-dependent processes relating to metals dissolution that affect OP_{ws}^{DTT}, here we focus mainly on OP_{wi}^{DTT}. Note that the MOUDI samples shown in Figure 4 at GT and RS sites were collected in different time periods. As is common, OC and EC had bimodal distributions with a larger accumulation-mode peak and a smaller peak in the coarse mode. Total Cu was most abundant in the coarse mode (data not shown, see Fang et al.[55]), consistent with insoluble Cu particles mainly emitted from mechanical generation, such as braking components and resuspended dust.[66,67] Compared to total Cu, water-soluble Cu peaked at a smaller size, which can be explained by a combination of primary emissions (i.e., brake wear) and secondary processing by sulfate particles forming acidic conditions.[55,68] Our previous paper[55] showed that sulfate can produce highly acidic fine aerosols capable of dissolving Cu emitted in an insoluble form, and this acid-dissolved Cu played an important role in shaping the distribution of OP_{ws}^{DTT}. It is noted that Mn is also an important transition metal ion contributing to OP_{ws}^{DTT}.[58,69] Since Mn had a size distribution similar to that of Cu, [55] Mn may be involved the same processes in shaping the distribution of OP_{ws}^{DTT}. In addition to water-soluble metals, other evidence points to organic species from combustion playing an important role in fine-mode OP_{ws}^{DTT} (~60% from organics and 40% from metals).[69] Thus,

contributions from both water-soluble metals and organic species can explain why OP^{DTT}_{ws} had a broad distribution that peaked between fine-mode OC and water-soluble Cu (Figure 4e, f). The variation in GMD at the roadside OP^{DTT}_{ws} can also be attributed to the varying relative contribution from water-soluble Cu and organic species; for example, higher concentration of Cu may shift the distribution toward the coarse mode.

Bimodal OP^{DTT}_{wi} follow distributions of insoluble species in the accumulation and coarse modes. A main insoluble fine-mode aerosol is soot (or EC). Figure 4c, d shows that measured EC mass size distributions converted to EC surface area distributions match well with OP^{DTT}_{wi} , consistent with OP^{DTT}_{wi} being associated with the EC surface. Note that OC and EC have similar surface area distributions (Figure S2), but much of OC is soluble, so it is difficult to infer insoluble OC size distributions from this data. We will show below that some of this insoluble OC, e.g., quinones or similar compounds, appear to coat soot. Studies reporting oxidation of PAHs[24] and diesel exhaust soot or black carbon[15,16,25] by ozone, forming surface-bound quinones and increasing OP^{DTT}, are consistent with our fine-mode OP^{DTT}_{wi} being associated with surfaces of EC. Measurements of fine-mode particle-bound PAHs in Atlanta traffic were highly correlated with black carbon ($r = 0.86$).[70] Furthermore, fine-mode number distributions of solid particles that remain insoluble when ambient aerosol was collected in water were highly correlated with EC mass concentrations[71] and had size distributions similar to that of EC (Figure S5), consistent with EC being the main insoluble fine-mode species.

The data also show the importance of time for atmospheric aging on fine-mode OP^{DTT}_{wi}. This can be seen by comparing the OP^{DTT}_{wi}/EC surface area ratio at the RS site, which is heavily influenced by primary emissions, to the GT site of more atmospheric processed aerosols. Fine-mode ($D_p < 1\ \mu m$) OP^{DTT}_{wi} per EC surface area concentration values were 4–5 times higher at the GT site (mean of OP^{DTT}_{wi} per EC surface area (mean ± standard deviation) was $(1.5 \pm 0.6) \times 10^{-8}$ and $(3.2 \pm 1.6) \times 10^{-9}$ nmol min^{-1} μm^{-2} for GT and RS sites, respectively; see Figures S6 and S7). A longer study also shows higher OP^{DTT}_{wi} per EC concentrations at the GT site based on bulk $PM_{2.5}$ samples collected simultaneously at both sites (Figure S8). This is consistent with PAH-coated EC being emitted by the road, but requiring oxidation to convert EC-surface PAHs to quinones. Higher O_3 levels away from the road due to less NO_x titration may also play a role. These processes explain the observed similar fine-mode OP^{DTT}_{wi} levels when measured simultaneously at the roadside and urban sites (Figure 3a). Because fresh soot per mass (or surface area) does not have as high OP^{DTT} as aged aerosol, OP^{DTT} is clearly not related solely to a soot surface property formed during emission.

Soluble transition metals also contribute to OP^{DTT}, but are typically not found in particles smaller than 1 μm. However, they may account for much of the coarse-mode OP^{DTT}_{wi}. Primary coarse-mode particles are generated by mechanical processes. There is limited

information on which chemical species may contribute to coarse-mode OP_{wi}^{DTT}, but the $CaCO_3$ surface area distribution is seen to be similar to coarse-mode OP_{wi}^{DTT} at both sites, suggesting that it is also related to a surface property. Soluble metals (and possibly some contribution from adsorbed EC and quinones; see Figure S9 and S10 for EC and OC in the coarse mode) may remain bound to these large mineral dust particles during the water extraction process and account for at least some of the coarse-mode OP_{wi}^{DTT}.

Intrinsic OP Distributions

Comparing the oxidative activity of different size particles on a per PM mass basis (intrinsic activity) can provide a measure of aerosol toxicity. Figure 5 shows that both OP_{ws}^{DTT} and OP_{wi}^{DTT} per mass are highest for quasi-ultrafine particles where the mass is low. [Note that OP^{DTT} per mass is also high for the large particles, but in this case masses may be underestimated due to inferring total $CaCO_3$ from soluble measured Ca^{2+}.] In terms of modes, OP_{ws}^{DTT} per mass was the highest for quasi-ultrafine, in agreement with some other studies.[53,54] OP_{wi}^{DTT} also had the highest per mass activity for the quasi-ultrafine mode, consistent with high soot (EC) toxicity. Although the intrinsic activities provide contrast in the OP potency of particles of differing sizes, overall potential for adverse health effects depends on exposure; the OP activity per volume of air, which has a very different distribution than that of per PM mass, and the efficiency of particle deposition as a function of size in the respiratory system.

Respiratory OP Deposition

Particle deposition patterns in the respiratory tract depend, in part, on particle size. Since chemical components driving OP_{wi}^{DTT} and OP_{ws}^{DTT} vary with particle size, different components of OP^{DTT} will be deposited in different regions. OP^{DTT} deposition was calculated for the whole respiratory tract (extrathoracic and all lung compartments) and two sub-regions (the extrathoracic compartment and the alveolar). In each region we compare the relative importance of OP^{DTT} associated with quasi-ultrafine, accumulation, and coarse modes. The results are shown in Figure 6. For the whole respiratory tract, coarse-mode OP_{wi}^{DTT} (DTT loss rate per volume of air) deposition dominated at both the GT and RS sites, accumulation-mode OP_{wi}^{DTT} deposition was also high, and quasi-ultrafine OP^{DTT} was minimal. For OP_{ws}^{DTT} a similar pattern was found, except accumulation-mode particles made greater contributions or were on par with coarse-mode particle contributions to whole respiratory tract deposition. Extrathoracic deposition patterns for both forms of OP^{DTT} were similar to those of the whole respiratory tract, and accumulation and coarse particles made the most contributions; coarse mode was larger for OP_{wi}^{DTT}, and coarse and accumulation were similar for OP_{ws}^{DTT}. For alveolar deposition, there was much less contribution from coarse-mode particles (coarse particle alveolar deposition was <4% of the whole respiratory

tract deposition), because the majority was deposited in the upper respiratory tract. Alveolar deposition was dominated by accumulation-mode particles for both OP_{wi}^{DTT} and OP_{ws}^{DTT}.

These comparisons show that, although quasi-ultrafine particles are more DTT-active per mass and are deposited in the alveoli with higher efficiencies than accumulation and coarse particles (close to 100%), the deposition levels of quasi-ultrafine OP-containing particles were small in this study, and so less important. These results are as expected; coarse-mode particles are deposited in the upper respiratory tract (extra-thoracic and tracheobronchial regions) and accumulation-mode particles predominantly in the alveoli. Consequently, upper respiratory deposition of OP_{wi}^{DTT} would be related to soluble metals, with minor contributions from quinones adsorbed to dust (or quinones adsorbed to soot adsorbed to dust). Similarly, for upper airway deposition of OP_{ws}^{DTT}, soluble transition metals would dominate.[55] For alveolar deposition of OP_{wi}^{DTT}, the main aerosol components would be those associated with, or adsorbed to, soot surfaces, the latter mostly quinones (or similar compounds). Alveolar deposition of OP_{ws}^{DTT} is also mainly associated with quinones; soluble transition metal ions would play a minor role.[55] Limited mixing between the organic aerosol (e.g., quinones) and transition metal ions in single particles due to association with different sizes (e.g., for $PM_{2.5}$, mixing is only likely in the 1–2.5 μm size range) raises the question if these main components of OP^{DTT} will extensively interact when deposited in the lung. Bulk measurements of OP^{DTT} that mix components of all sizes for $PM_{2.5}$ samples may produce interactions between DTT-active organic species and transition metal ions that would not occur to the same extent in lung lining fluid, leading to artifacts. Finally, it remains to be determined if water-soluble and water-insoluble OP^{DTT} are linked to differing health end points, despite both forms of OP^{DTT} being driven by similar size-dependent aerosol chemical components.

Supplementary Material

Refer to Web version on PubMed Central for supplementary material.

Acknowledgments

This work was supported by the U.S. Environmental Protection Agency under grant number RD834799. The contents are solely the responsibility of the grantee and do not necessarily represent the official views of the U.S. EPA. Further, U.S. EPA does not endorse the purchase of any commercial products or services mentioned in the work. The findings and conclusions in this report are those of the authors and do not necessarily represent the views of the National Institute for Occupational Safety and Health. The authors thank Emily M. Saad for helping in running ICP-MS for the MOUDI samples, and Mike Bergin and Roby Greenwald for providing the water-insoluble particle size distributions. T.F. acknowledges support from the Oversea Study Program of Guangzhou Elite Project.

References

1. Hoek G, Krishnan RM, Beelen R, Peters A, Ostro B, Brunekreef B, Kaufman JD. Long-term air pollution exposure and cardio- respiratory mortality: a review. Environ Health. 2013; 12(1):1–16. [PubMed: 23286340]
2. Brook RD, Rajagopalan S, Pope CA, Brook JR, Bhatnagar A, Diez-Roux AV, Holguin F, Hong Y, Luepker RV, Mittleman MA, Peters A, Siscovick D, Smith SC, Whitsel L, Kaufman JD. on behalf of the American Heart Association Council on, E., Prevention, C. o. t. K. i. C. D., Council on

Nutrition, PA. Metabolism, Particulate matter air pollution and cardiovascular disease: an update to the scientific statement from the American heart association. Circulation. 2010; 121(21):2331–2378. [PubMed: 20458016]

3. Pope CA, Burnett RT, Thurston GD, Thun MJ, Calle EE, Krewski D, Godleski JJ. Cardiovascular mortality and long-term exposure to particulate air pollution: epidemiological evidence of general pathophysiological pathways of disease. Circulation. 2004; 109(1):71–77. [PubMed: 14676145]
4. Xia T, Kovochich M, Brant J, Hotze M, Sempf J, Oberley T, Sioutas C, Yeh JI, Wiesner MR, Nel AE. Comparison of the abilities of ambient and manufactured nanoparticles to induce cellular toxicity according to an oxidative stress paradigm. Nano Lett. 2006; 6(8):1794–1807. [PubMed: 16895376]
5. Yang A, Janssen NA, Brunekreef B, Cassee FR, Hoek G, Gehring U. Children's respiratory health and oxidative potential of PM2.5: the PIAMA birth cohort study. Occup Environ Med. 2016; 73(3): 154–60. [PubMed: 26755634]
6. Bates JT, Weber RJ, Abrams J, Verma V, Fang T, Klein M, Strickland MJ, Sarnat SE, Chang HH, Mulholland JA, Tolbert PE, Russell AG. Reactive Oxygen Species Generation Linked to Sources of Atmospheric Particulate Matter and Cardiorespiratory Effects. Environ Sci Technol. 2015; 49(22): 13605–13612. [PubMed: 26457347]
7. Delfino RJ, Staimer N, Tjoa T, Gillen DL, Schauer JJ, Shafer MM. Airway inflammation and oxidative potential of air pollutant particles in a pediatric asthma panel. J Exposure Sci Environ Epidemiol. 2013; 23:466–473.
8. Weichenthal S, Crouse DL, Pinault L, Godri-Pollitt K, Lavigne E, Evans G, van Donkelaar A, Martin RV, Burnett RT. Oxidative burden of fine particulate air pollution and risk of cause-specific mortality in the Canadian Census Health and Environment Cohort (CanCHEC). Environ Res. 2016; 146:92–99. [PubMed: 26745732]
9. Weichenthal S, Lavigne E, Evans G, Pollitt K, Burnett RT. Ambient PM(2.5) and risk of emergency room visits for myocardial infarction: impact of regional PM(2.5) oxidative potential: a case-crossover study. Environ Health. 2016; 15:46. [PubMed: 27012244]
10. Strak M, Janssen NA, Godri KJ, Gosens I, Mudway IS, Cassee FR, Lebret E, Kelly FJ, Harrison RM, Brunekreef B, Steenhof M, Hoek G. Respiratory health effects of airborne particulate matter: the role of particle size, composition, and oxidative potential-the RAPTES project. Environ Health Perspect. 2012; 120(8):1183–9. [PubMed: 22552951]
11. Steenhof M, Mudway IS, Gosens I, Hoek G, Godri KJ, Kelly FJ, Harrison RM, Pieters RHH, Cassee FR, Lebret E, Brunekreef BA, Strak M, Janssen NAH. Acute nasal pro-inflammatory response to air pollution depends on characteristics other than particle mass concentration or oxidative potential: the RAPTES project. Occup Environ Med. 2013; 70(5):341. [PubMed: 23428835]
12. Atkinson RW, Samoli E, Analitis A, Fuller GW, Green DC, Anderson HR, Purdie E, Dunster C, Aitlhadj L, Kelly FJ, Mudway IS. Short-term associations between particle oxidative potential and daily mortality and hospital admissions in London. Int J Hyg Environ Health. 2016; 219(6):566–572. [PubMed: 27350257]
13. Fang T, Verma V, Bates JT, Abrams J, Klein M, Strickland MJ, Sarnat SE, Chang HH, Mulholland JA, Tolbert PE, Russell AG, Weber RJ. Oxidative potential of ambient water-soluble PM2.5 in the southeastern United States: contrasts in sources and health associations between ascorbic acid (AA) and dithiothreitol (DTT) assays. Atmos Chem Phys. 2016; 16(6):3865–3879.
14. Daher N, Ning Z, Cho AK, Shafer M, Schauer JJ, Sioutas C. Comparison of the chemical and oxidative characteristics of particulate matter (PM) collected by different methods: filters, impactors, and biosamplers. Aerosol Sci Technol. 2011; 45(11):1294–1304.
15. McWhinney RD, Badali K, Liggio J, Li S-M, Abbatt JPD. Filterable redox cycling activity: a comparison between diesel exhaust particles and secondary organic aerosol constituents. Environ Sci Technol. 2013; 47(7):3362–3369. [PubMed: 23470039]
16. Li Q, Shang J, Zhu T. Physicochemical characteristics and toxic effects of ozone-oxidized black carbon particles. Atmos Environ. 2013; 81:68–75.
17. Yang A, Jedynska A, Hellack B, Kooter I, Hoek G, Brunekreef B, Kuhlbusch TAJ, Cassee FR, Janssen NAH. Measurement of the oxidative potential of PM2.5 and its constituents: The effect of extraction solvent and filter type. Atmos Environ. 2014; 83:35–42.

18. Verma V, Rico-Martinez R, Kotra N, King LE, Liu J, Snell TW, Weber RJ. Contribution of water-soluble and insoluble components and their hydrophobic/hydrophilic subfractions to the reactive oxygen species-generating potential of fine ambient aerosols. Environ Sci Technol. 2012; 46(20): 11384–11392. [PubMed: 22974103]
19. McCreanor J, Cullinan P, Nieuwenhuijsen MJ, Stewart-Evans J, Malliarou E, Jarup L, Harrington R, Svartengren M, Han I-K, Ohman-Strickland P, Chung KF, Zhang J. Respiratory effects of exposure to diesel traffic in persons with asthma. N Engl J Med. 2007; 357(23):2348–2358. [PubMed: 18057337]
20. Grahame TJ, Schlesinger RB. Cardiovascular health and particulate vehicular emissions: a critical evaluation of the evidence. Air Qual, Atmos Health. 2010; 3(1):3–27. [PubMed: 20376169]
21. Janssen, NA., Gerlofs-Nijland, ME., Lanki, T., Salonen, RO., Cassee, F., Hoek, G., Fischer, P., Brunekreef, B., Krzyzanowski, M. Health effects of black carbon. World Health Organization; Denmark: 2012.
22. Homann K-H. Fullerenes and soot formation—new pathways to large particles in flames. Angew Chem, Int Ed. 1998; 37(18):2434–2451.
23. Shiraiwa M, Sosedova Y, Rouvière A, Yang H, Zhang Y, Abbatt JPD, Ammann M, Pöschl U. The role of long-lived reactive oxygen intermediates in the reaction of ozone with aerosol particles. Nat Chem. 2011; 3(4):291–295. [PubMed: 21430687]
24. Antinolo M, Willis MD, Zhou S, Abbatt JPD. Connecting the oxidation of soot to its redox cycling abilities. Nat Commun. 2015; 6:6812. [PubMed: 25873384]
25. McWhinney RD, Gao SS, Zhou S, Abbatt JPD. Evaluation of the effects of ozone oxidation on redox-cycling activity of two-stroke engine exhaust particles. Environ Sci Technol. 2011; 45(6): 2131–2136. [PubMed: 21341691]
26. Pan C-JG, Schmitz DA, Cho AK, Froines J, Fukuto JM. Inherent redox properties of diesel exhaust particles: catalysis of the generation of reactive oxygen species by biological reductants. Toxicol Sci. 2004; 81(1):225–232. [PubMed: 15201441]
27. Sauvain J-J, Rossi MJ, Riediker M. Comparison of three acellular tests for assessing the oxidation potential of nanomaterials. Aerosol Sci Technol. 2013; 47(2):218–227.
28. Dellinger B, Lomnicki S, Khachatryan L, Maskos Z, Hall RW, Adounkpe J, McFerrin C, Truong H. Formation and stabilization of persistent free radicals. Proc Combust Inst. 2007; 31(1):521–528. [PubMed: 25598747]
29. Arangio AM, Tong H, Socorro J, Pöschl U, Shiraiwa M. Quantification of environmentally persistent free radicals and reactive oxygen species in atmospheric aerosol particles. Atmos Chem Phys. 2016; 16(20):13105–13119.
30. Ostro BD, Hurley S, Lipsett MJ. Air pollution and daily mortality in the coachella valley, california: a study of PM10 dominated by coarse particles. Environ Res. 1999; 81(3):231–238. [PubMed: 10585019]
31. Osornio-Vargas AR, Serrano J, Rojas-Bracho L, Miranda J, Garcia-Cuellar C, Reyna MA, Flores G, Zuk M, Quintero M, Vazquez I, Sanchez-Perez Y, Lopez T, Rosas I. In vitro biological effects of airborne PM(2.5) and PM(10) from a semi-desert city on the Mexico-US border. Chemosphere. 2011; 83(4):618–26. [PubMed: 21168895]
32. Hetland RB, Cassee FR, Refsnes M, Schwarze PE, Låg M, Boere AJF, Dybing E. Release of inflammatory cytokines, cell toxicity and apoptosis in epithelial lung cells after exposure to ambient air particles of different size fractions. Toxicol In Vitro. 2004; 18(2):203–212. [PubMed: 14757111]
33. Shirmohammadi F, Hasheminassab S, Wang D, Saffari A, Schauer JJ, Shafer MM, Delfino RJ, Sioutas C. Oxidative potential of coarse particulate matter (PM10–2.5) and its relation to water solubility and sources of trace elements and metals in the Los Angeles Basin. Environ Sci: Processes Impacts. 2015; 17(12):2110–2121.
34. Furusjö E, Sternbeck J, Cousins AP. PM10 source characterization at urban and highway roadside locations. Sci Total Environ. 2007; 387(1–3):206–219. [PubMed: 17822744]
35. Weinbruch S, Worringen A, Ebert M, Scheuvens D, Kandler K, Pfeffer U, Bruckmann P. A quantitative estimation of the exhaust, abrasion and resuspension components of particulate traffic emissions using electron microscopy. Atmos Environ. 2014; 99:175–182.

36. Dana, JD. Manual of mineral science. 23. Klein, C., Dutrow, B., editors. Wiley; Hoboken, NJ: 2008.
37. Schoonen MAA, Cohn CA, Roemer E, Laffers R, Simon SR, O'Riordan T. Mineral-induced formation of reactive oxygen species. Rev Mineral Geochem. 2006; 64(1):179.
38. Peters A, Wichmann H, Tuch T, Heinrich J, Heyder J. Respiratory effects are associated with the number of ultrafine particles. Am J Respir Crit Care Med. 1997; 155:1376–1383. [PubMed: 9105082]
39. Lippmann, M. Comprehensive Physiology. John Wiley & Sons, Inc; New York: 2010. Regional deposition of particles in the human respiratory tract.
40. Nemmar A, Hoet PHM, Vanquickenborne B, Dinsdale D, Thomeer M, Hoylaerts MF, Vanbilloen H, Mortelmans L, Nemery B. Passage of inhaled particles into the blood circulation in humans. Circulation. 2002; 105(4):411. [PubMed: 11815420]
41. Furuyama A, Kanno S, Kobayashi T, Hirano S. Extrapulmonary translocation of intratracheally instilled fine and ultrafine particles via direct and alveolar macrophage-associated routes. Arch Toxicol. 2009; 83(5):429–437. [PubMed: 18953527]
42. De Jong WH, Hagens WI, Krystek P, Burger MC, Sips AJ, Geertsma RE. Particle size-dependent organ distribution of gold nanoparticles after intravenous administration. Biomaterials. 2008; 29(12):1912–9. [PubMed: 18242692]
43. Li X-Y, Hao L, Liu Y-H, Chen C-Y, Pai VJ, Kang JX. Protection against fine particle-induced pulmonary and systemic inflammation by omega-3 polyunsaturated fatty acids. Biochim Biophys Acta, Gen Subj. 2017; 1861(3):577–584.
44. Oberdorster G, Sharp Z, Atudorei V, Elder A, Gelein R, Lunts A, Kreyling W, Cox C. Extrapulmonary translocation of ultrafine carbon particles following whole-body inhalation exposure of rats. J Toxicol Environ Health, Part A. 2002; 65(20):1531–1543. [PubMed: 12396867]
45. Oberdorster G, Sharp Z, Atudorei V, Elder A, Gelein R, Kreyling W, Cox C. Translocation of inhaled ultrafine particles to the brain. Inhalation Toxicol. 2004; 16(6–7):437–45.
46. Maher BA, Ahmed IAM, Karloukovski V, MacLaren DA, Foulds PG, Allsop D, Mann DMA, Torres-Jardón R, Calderon-Garciduenas L. Magnetite pollution nanoparticles in the human brain. Proc Natl Acad Sci U S A. 2016; 113(39):10797. [PubMed: 27601646]
47. Chen H, Kwong JC, Copes R, Tu K, Villeneuve PJ, van Donkelaar A, Hystad P, Martin RV, Murray BJ, Jessiman B, Wilton AS, Kopp A, Burnett RT. Living near major roads and the incidence of dementia, Parkinson's disease, and multiple sclerosis: a population-based cohort study. Lancet. 2017; 389:718–726. [PubMed: 28063597]
48. Sunyer J, Esnaola M, Alvarez-Pedrerol M, Forns J, Rivas I, Lopez-Vicente M, Suades-Gonzalez E, Foraster M, Garcia-Esteban R, Basagana X, Viana M, Cirach M, Moreno T, Alastuey A, Sebastian-Galles N, Nieuwenhuijsen M, Querol X. Association between traffic-related air pollution in schools and cognitive development in primary school children: a prospective cohort study. PLoS Med. 2015; 12(3):e1001792. [PubMed: 25734425]
49. De Haar C, Hassing I, Bol M, Bleumink R, Pieters R. Ultrafine but not fine particulate matter causes airway inflammation and allergic airway sensitization to co-administered antigen in mice. Clin Exp Allergy. 2006; 36(11):1469–1479. [PubMed: 17083358]
50. Delfino RJ, Staimer N, Tjoa T, Gillen DL, Polidori A, Arhami M, Kleinman MT, Vaziri ND, Longhurst J, Sioutas C. Air pollution exposures and circulating biomarkers of effect in a susceptible population: clues to potential causal component mixtures and mechanisms. Environ Health Perspect. 2009; 117(8):1232–1238. [PubMed: 19672402]
51. Li N, Sioutas C, Cho AK, Schmitz D, Misra C, Sempf J, Wang M, Oberley T, Froines J, Nel A. Ultrafine particulate pollutants induce oxidative stress and mitochondrial damage. Environ Health Perspect. 2003; 111(4):455–460. [PubMed: 12676598]
52. Steenhof M, Gosens I, Strak M, Godri KJ, Hoek G, Cassee FR, Mudway IS, Kelly FJ, Harrison RM, Lebret E, Brunekreef B, Janssen NAH, Pieters RHH. In vitro toxicity of particulate matter (PM) collected at different sites in the Netherlands is associated with PM composition, size fraction and oxidative potential–the RAPTES project. Part Fibre Toxicol. 2011; 8:26. [PubMed: 21888644]

53. Cho AK, Sioutas C, Miguel AH, Kumagai Y, Schmitz DA, Singh M, Eiguren-Fernandez A, Froines JR. Redox activity of airborne particulate matter at different sites in the Los Angeles Basin. Environ Res. 2005; 99(1):40–47. [PubMed: 16053926]
54. Ntziachristos L, Froines JR, Cho AK, Sioutas C. Relationship between redox activity and chemical speciation of size-fractionated particulate matter. Part Fibre Toxicol. 2007; 4(1):5. [PubMed: 17555562]
55. Fang T, Guo H, Zeng L, Verma V, Nenes A, Weber RJ. Highly acidic ambient particles, soluble metals, and oxidative potential: a link between sulfate and aerosol toxicity. Environ Sci Technol. 2017; 51:2611–2620. [PubMed: 28141928]
56. Sauvain J-J, Deslarzes S, Storti F, Riediker M. Oxidative Potential of Particles in Different Occupational Environments: A Pilot Study. Ann Occup Hyg. 2015; 59(7):882–894. [PubMed: 25846363]
57. Chow JC, Watson JG, Chen LWA, Chang MCO, Robinson NF, Trimble D, Kohl S. The IMPROVE_A Temperature Protocol for Thermal/Optical Carbon Analysis: Maintaining Consistency with a Long-Term Database. J Air Waste Manage Assoc. 2007; 57(9):1014–1023.
58. Verma V, Fang T, Guo H, King LE, Bates JT, Peltier RE, Edgerton ES, Russell AG, Weber RJ. Reactive oxygen species associated with water-soluble PM2.5 in the southeastern United States: spatiotemporal trends and source apportionment. Atmos Chem Phys. 2014; 14(23):12915–12930.
59. Turpin BJ, Lim H-J. Species contributions to PM2.5 mass concentrations: revisiting common assumptions for estimating organic mass. Aerosol Sci Technol. 2001; 35(1):602–610.
60. Tang MJ, Whitehead J, Davidson NM, Pope FD, Alfarra MR, McFiggans G, Kalberer M. Cloud condensation nucleation activities of calcium carbonate and its atmospheric ageing products. Phys Chem Chem Phys. 2015; 17(48):32194–32203. [PubMed: 26578034]
61. Zhao Y, Chen Z, Shen X, Huang D. Heterogeneous reactions of gaseous hydrogen peroxide on pristine and acidic gas-processed calcium carbonate particles: Effects of relative humidity and surface coverage of coating. Atmos Environ. 2013; 67:63–72.
62. Fang T, Verma V, Guo H, King LE, Edgerton ES, Weber RJ. A semi-automated system for quantifying the oxidative potential of ambient particles in aqueous extracts using the dithiothreitol (DTT) assay: results from the Southeastern Center for Air Pollution and Epidemiology (SCAPE). Atmos Meas Tech. 2015; 8(1):471–482.
63. Oakes M, Ingall ED, Lai B, Shafer MM, Hays MD, Liu ZG, Russell AG, Weber RJ. Iron solubility related to particle sulfur content in source emission and ambient fine particles. Environ Sci Technol. 2012; 46(12):6637–6644. [PubMed: 22621615]
64. Longo AF, Vine DJ, King LE, Oakes M, Weber RJ, Huey LG, Russell AG, Ingall ED. Composition and oxidation state of sulfur in atmospheric particulate matter. Atmos Chem Phys. 2016; 16(21): 13389–13398.
65. ICRP. Publication 66: Human Respiratory Tract Model for Radiological Protection. Pergamon; Oxford, UK: 1994. p. 36-52.
66. Adachi K, Tainosho Y. Characterization of heavy metal particles embedded in tire dust. Environ Int. 2004; 30(8):1009–1017. [PubMed: 15337346]
67. Garg BD, Cadle SH, Mulawa PA, Groblicki PJ, Laroo C, Parr GA. Brake wear particulate matter emissions. Environ Sci Technol. 2000; 34(21):4463–4469.
68. Fang T, Guo H, Verma V, Peltier RE, Weber RJ. PM2.5 water-soluble elements in the southeastern United States: automated analytical method development, spatiotemporal distributions, source apportionment, and implications for heath studies. Atmos Chem Phys. 2015; 15(20):11667–11682.
69. Verma V, Fang T, Xu L, Peltier RE, Russell AG, Ng NL, Weber RJ. Organic aerosols associated with the generation of Reactive Oxygen Species (ROS) by water-soluble PM2.5. Environ Sci Technol. 2015; 49(7):4646–4656. [PubMed: 25748105]
70. Greenwald R, Bergin MH, Yip F, Boehmer T, Kewada P, Shafer MM, Schauer JJ, Sarnat JA. On-roadway in-cabin exposure to particulate matter: measurement results using both continuous and time-integrated sampling approaches. Aerosol Sci Technol. 2014; 48(6):664–675.
71. Greenwald R, Bergin MH, Weber R, Sullivan A. Size-resolved, real-time measurement of water-insoluble aerosols in metropolitan Atlanta during the summer of 2004. Atmos Environ. 2007; 41(3):519–531.

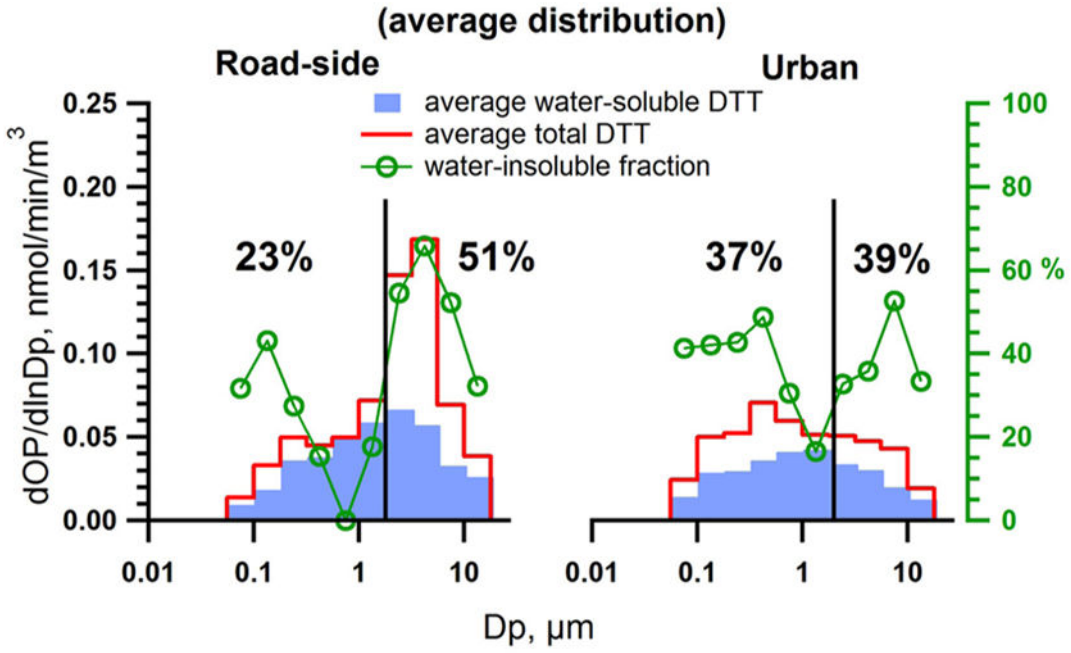

Figure 1.

Average distribution of total and water-soluble DTT activities from all MOUDI samples. The mean water-insoluble fractions were calculated from the average distribution for fine and coarse modes separated by the vertical line at aerodynamic diameter D_p = 1.8 μm.

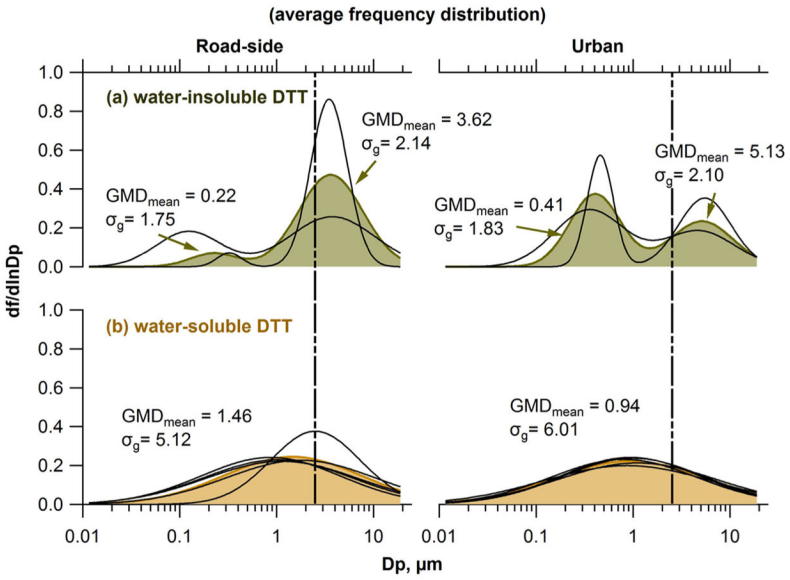

Figure 2.

Averaged frequency distributions of (a) water-insoluble DTT and (b) water-soluble DTT activities at a roadside site (RS, left panels) and an urban background (GT, right panels) in Atlanta, GA, USA. The vertical dotted line is aerodynamic diameter D_p = 2.5 μm. GMD_{mean} and σ_g are the mean of the fit geometric mean diameter (μm) and geometric standard deviation, respectively, of multiple MOUDI samples (two sets for water-insoluble DTT, five sets for water-soluble DTT, per volume of air). Shaded color represents the mean frequency distribution. Each black curve represents the frequency distribution from each MOUDI measurement. The equation for the frequency distribution can be found in the Supporting Information.

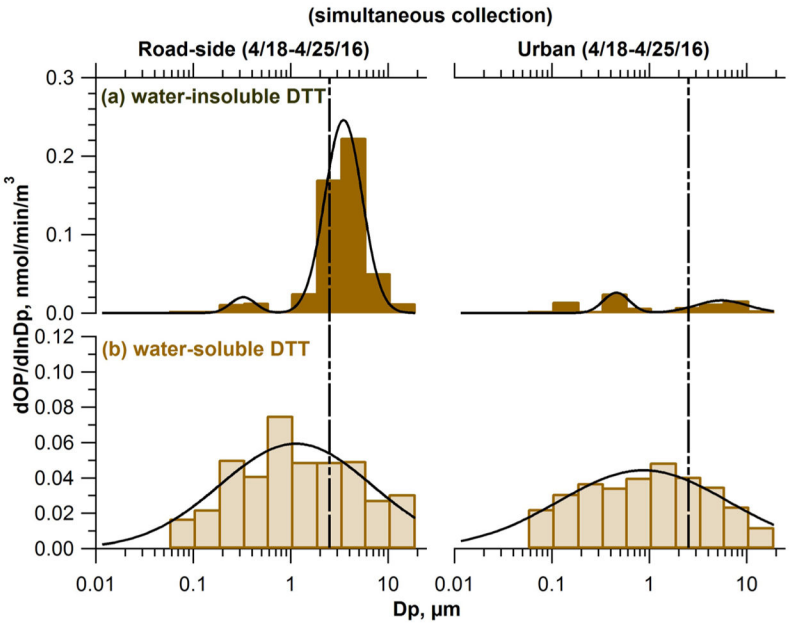

Figure 3.

Ambient size distribution of water-insoluble (a) and -soluble (b) oxidative potential from MOUDI samples collected simultaneously at a roadside site (RS, left panels) and a representative urban site (GT, right panels) in Atlanta, GA, USA. The vertical dotted line is aerodynamic diameter D_p = 2.5 μm.

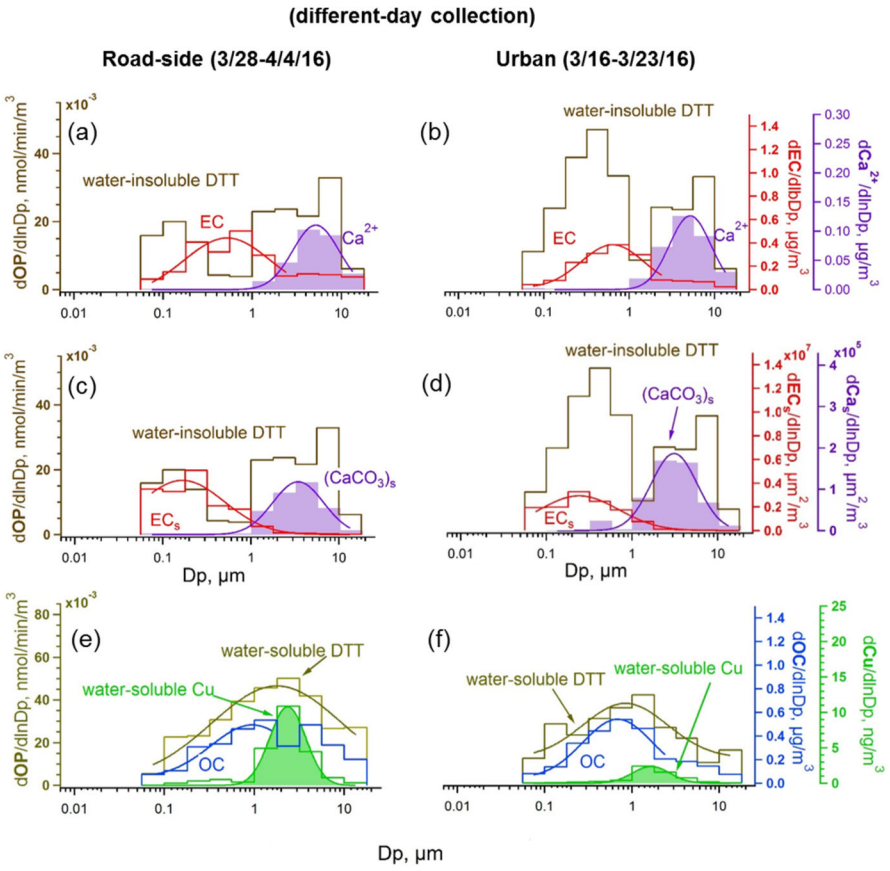

Figure 4.

Size distributions of chemical species and oxidative potential at a roadside site (RS, left panels, March 28–April 4, 2016) and a representative urban site (GT, right panels, March 16–23, 2016) in Atlanta, GA. EC_s and $(CaCO_3)_s$ in (c) and (d) represent surface area distributions of EC and estimated $CaCO_3$; others (a, b, e, f) are mass distributions.

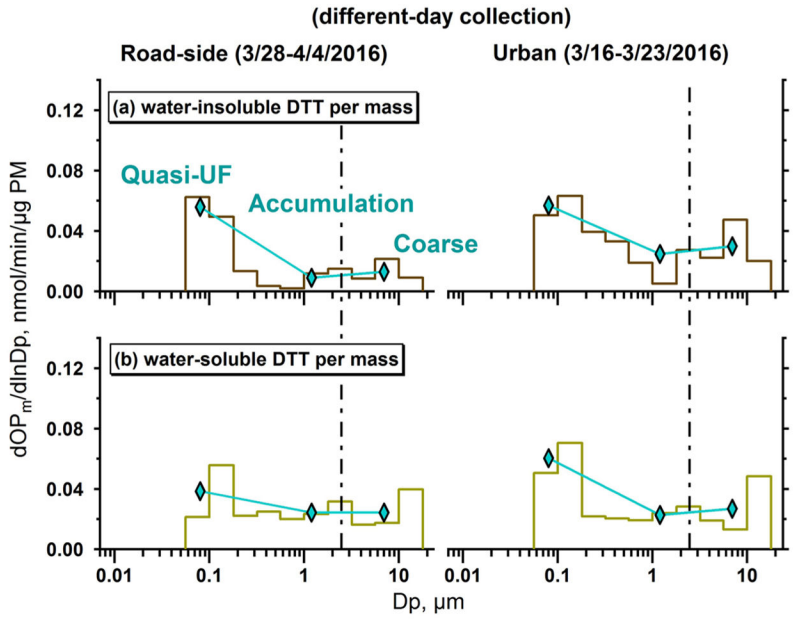

Figure 5.

Water-insoluble (a) and -soluble (b) oxidative potential distributions on a per PM mass basis at a roadside site (RS, left panels, March 28–April 4, 2016) and a representative urban site (GT, right panels, March 16–23, 2016) in Atlanta, GA, USA. Average OP per mass for three modes, quasi-ultrafine (<0.18 μm), accumulation (0.18 ≤ D_p ≤ 3.2 μm), and coarse (3.2 < D_p < 10 μm) is also shown (diamonds with line). PM mass on each MOUDI stage was estimated from the sum of measured chemical components. The dotted line is aerodynamic diameter D_p = 2.5 μm.

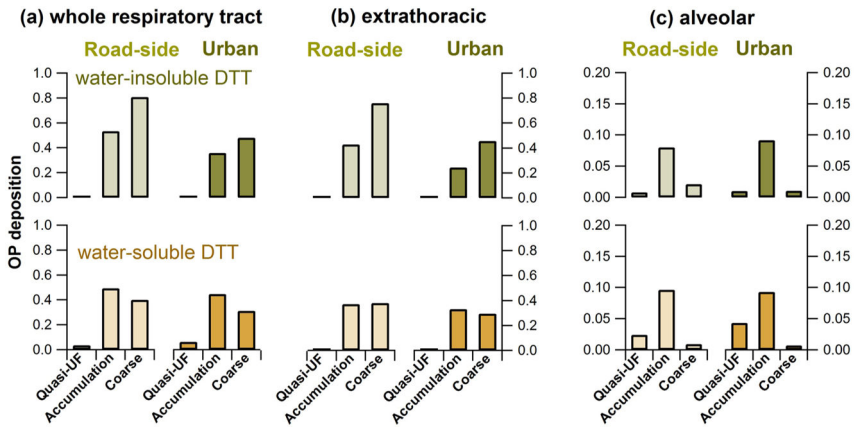

Figure 6.

Estimated whole respiratory tract (a), extrathoracic (b), and alveolar (c) deposition of PM oxidative potential in the human respiratory system for three aerosol size modes: quasi-ultrafine ($D_p < 0.18$ μm), accumulation ($0.18 \leq D_p \leq 3.2$ μm), and coarse ($3.2 < D_p < 10$ μm). Whole-lung deposition refers to the total OP deposited in the whole respiratory tract. Deposition of OP equals the deposition efficiency times the average OP frequency distribution (vertical axis is unitless), both a function of particle size. Deposition efficiencies were based on an empirical expression assuming unit density spheres for steady breathing with a flow rate of 1.5 $cm^3\ h^{-1}$, breathing frequency of 20 min^{-1}, and tidal volume of 1500 cm^3. OP deposition on the vertical axis was calculated by integrating the deposition of OP over the three particle size modes.